Journal of Colloid and Interface Science 566 (2020) 304–315

Contents lists available at ScienceDirect

Journal of Colloid and Interface Science

journal homepage: www.elsevier.com/locate/jcis

Unexpected conformational behavior of poly(poly(ethylene glycol) methacrylate)-poly(propylene carbonate)-poly(poly(ethylene glycol) methacrylate) (PPEGMA-PPC-PPEGMA) amphiphilic block copolymers in micellar solution and at the air-water interface

Jaewon Lee [a], Jingyi Pan [b], Jaehun Chun [c], You-Yeon Won [b,*]

[a] Department of Biomedical, Biological and Chemical Engineering, University of Missouri, Columbia, MO 65211, USA
[b] Davidson School of Chemical Engineering, Purdue University, West Lafayette, IN 47907, USA
[c] Physical and Computational Sciences Directorate, Pacific Northwest National Laboratory, Richland, WA 99352, USA

GRAPHICAL ABSTRACT

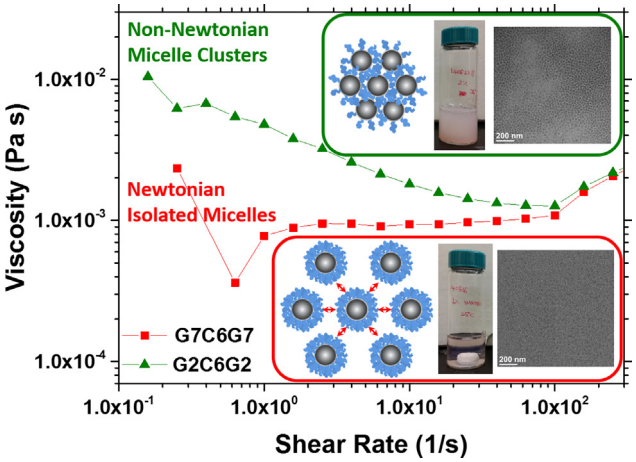

ARTICLE INFO

Article history:
Received 18 November 2019
Revised 3 January 2020
Accepted 3 January 2020
Available online 24 January 2020

Keywords:
Poly(poly(ethylene glycol) methacrylate) (PPEGMA)
Poly(propylene carbonate) (PPC)
Amphiphilic block copolymer

ABSTRACT

Hypothesis: This paper investigates the self-assembly behavior of a new amphiphilic block copolymer, PPEGMA-PPC-PPEGMA, in dilute aqueous solution and at the air–water interface. In PPEGMA-PPC-PPEGMA, the hydrophilic PEG moieties exist as side chains attached to the PMA backbone. Because of this unique non-linear architecture, the morphological and conformational properties of self-assembled PPEGMA-PPC-PPEGMA polymers are expected to be different from those of conventional linear PEG-based polymer surfactants.

Experiments: For this study, three PPE**G**MA-PP**C**-PPE**G**MA samples having an identical PPC molecular weight (**5.6** kDa) and different PPEGMA molecular weights (**7.2**, **2.8** and **2.1** kDa on either side) (named "**G7C6G7**", "**G3C5G3**", and "**G2C6G2**", respectively) were synthesized. The micellar self-assembly behaviors of these materials were investigated by cryo-TEM, rheology, DLS, and visual observation. Langmuir

Abbreviations: PPEGMA, poly(poly(ethylene glycol) methacrylate); PPC, poly(propylene carbonate); PEG, poly(ethylene glycol); PMA, poly(methacrylate); RAFT, reversible addition fragmentation transfer; CPCP, 4-cyano-4-(phenylcarbonothioylthio)pentanoic acid; DLS, dynamic light scattering; Cryo-TEM, cryogenic transmission electron microscopy.

* Corresponding author at: Davidson School of Chemical Engineering, Purdue University, 480 Stadium Mall Drive, West Lafayette, IN 47907, USA.
E-mail address: yywon@ecn.purdue.edu (Y.-Y. Won).

https://doi.org/10.1016/j.jcis.2020.01.080
0021-9797/

Micelle
Cryogenic transmission electron microscopy (cryo-TEM)
Rheology
Langmuir monolayer
Surface pressure-area isotherm

monolayers of these materials were characterized by surface mechanical testing.
Findings: PPEGMA-PPC-PPEGMA micelles were found to have a spherical geometry, irrespective of copolymer composition. Interestingly, G2C6G2 and G3C6G3 micelles formed weakly-bound clusters, whereas G7C6G7 micelles predominantly existed as isolated micelles. Detailed analysis suggests that this unexpected trend in micelle morphology originates from the fact that the PPEGMA blocks are only partially hydrated at aqueous interfaces. Detailed features of the surface pressure-area isotherms obtained from Langmuir PPEG-PPC-PPEGMA monolayers further supported this notion.

1. Introduction

Poly(ethylene glycol)(PEG)-based amphiphilic block copolymers are used in many industrial applications, for instance, as detergents, dispersants, foaming agents, emulsifiers, gelling agents, and pharmaceutical excipients (enhancing drug bioavailability and controlled release) [1]. In dilute solutions, amphiphilic block copolymers form micelles. Based on their dynamic/preparation characteristics, block copolymer micelles can be grouped into three types: (1) equilibrium micelles formed by molecularly water-soluble block copolymers having finite (relatively high) critical micellization concentrations (CMCs) and thus capable of exchanging material between themselves (e.g., Poloxamer/Pluronic® [1], poly(ethylene glycol)-poly(lactic-*co*-glycolic acid) [2]); (2) globally non-equilibrium ("non-ergodic") micelles formed by simple hydration of molecularly insoluble block copolymers with zero CMC (poly(ethylene glycol)-poly(butadiene) [3,4]); (3) fully non-equilibrium (kinetically frozen) micelles of zero-CMC block copolymers that can only be produced via solvent exchange processing (e.g., poly(ethylene glycol)-poly(styrene) [5]). All three types of polymer micelles have been extensively studied. Regardless of polymer/micelle type, the morphology of block copolymer micelles is known to be primarily controlled by the relative sizes of the hydrophilic vs. hydrophobic blocks of the amphiphilic block copolymer; block copolymers with relatively high PEG block molecular weights prefer micelle structures with a high interfacial curvature (i.e., spherical micelles), and as the relative size of the PEG block is decreased, the preferred micelle shape shifts to cylindrical, and then to planar (i.e., vesicular/bilayered) [1,6–8]. The preferred interfacial curvature is determined by an interplay of (interfacial tension and) core/corona chain conformations, which are influenced by the (chemistries and) relative sizes of the hydrophilic and hydrophobic blocks [7].

Recently, a variant of the PEG chemistry, poly(poly(ethylene glycol) methacrylate)) (PPEGMA), has become popular for use as a hydrophilic component for amphiphilic block copolymers. The first report of a study of PPEGMA-based block copolymers dates back to early 2000 s [9]; PPEGMA has also been referred to as poly(oligo oxyethylene methacrylate) (POEM). Unlike linear PEG (which is typically synthesized by the stringent anionic polymerization method), monodisperse PPEGMA blocks can be conveniently synthesized using controlled radical polymerization mechanisms (such as atom transfer radical polymerization (ATRP) and reversible addition fragmentation transfer (RAFT)). A distinguishing feature of PPEGMA relative to linear PEG is that in the PPEGMA structure, PEG units are configured as side chains. PPEGMA homopolymers are known to be completely water soluble. However, the exact molecular conformations that the PEG side chains and the poly(methacrylate) (PMA) backbone chain would adopt within self-assembled structures formed in water by PPEGMA-based amphiphilic block copolymers (e.g., micelles) have not been fully elucidated. One might be tempted to assume that similarly to the PPEGMA homopolymer situation, the entire PPEGMA block would exist in a fully hydrated state even in a micellar system. Also, it is an unexplored question whether micelles formed by PPEGMA-based block copolymers would exhibit similar morphological trends to those seen in linear PEG-based block copolymer micelles (discussed above). These are the questions we attempt to address in the present article.

Specifically, in this work, we studied new amphiphilic triblock copolymers created by combining PPEGMA with poly(propylene carbonate) (PPC) (PPEGMA-PPC-PPEGMA). This material was chosen for the following reasons. Recently, PPC has attracted significant attention from researchers as a "green" material; PPC can be synthesized from a renewable resource, CO_2, and propylene oxide, and it readily degrades (back to CO_2 and other small compounds) upon heating [10,11] or via biological catalysis [12]. Monodisperse high molecular weight PPC can be synthesized, for instance, using a cobalt-salen catalyst [13]. As this work demonstrates, PPEGMA can be attached to PPC via RAFT. PPEGMA-PPC-PPEGMA has the potential to be used as an alternative to commercial linear PEG-based block copolymer surfactants (such as Poloxamers) with one advantage being that PPEGMA-PPC-PPEGMA is (bio)degradable and thus more environmentally friendly. Extensive studies would be required to establish similarities and differences between this and other conventional PEG-based polymer surfactants.

In this paper, we report our initial study of the conformational behavior of PPEGMA-PPC-PPEGMA triblock block copolymers in micelle solution and at the air–water interface. For this study, three PPEGMA-PPEC-PPEGMA materials having an identical PPC molecular weight and different PPEGMA molecular weights were prepared by RAFT polymerization of PEGMA from a dihydroxy PPC precursor. Micelles of these polymers could be produced by simple hydration. The structural and flow properties of these micelles were measured by DLS, cryo-TEM, and steady shear rheometry. Langmuir monolayers of these polymers could be prepared at the air–water interface by spreading with a volatile organic co-solvent. The surface pressure-area isotherms were measured on these monolayers. Combined results suggest that at aqueous-hydrophobic interfaces, the PPEGMA blocks are normally only partially hydrated with only the PEG side chains being hydrated and the PMA backbone remaining undissolved and collapsed at the interface in contact with the hydrophobic domain formed by PPC. At the air–water interface, the collapse of the insoluble monolayer formed by the PMA backbone segments during compression is manifested as a secondary plateau in the surface pressure-area isotherms of the PPEGMA-PPC-PPEGMA polymers. In micelle situations, an important consequence of the partial hydration of the PPEGMA block is that spherical micelles with short PPEGMA chains form van der Waals clusters because of insufficient steric protection provided by the low molecular weight PEG side chains. Interestingly, unlike linear PEG-based block copolymers, PPEGMA-PPC-PPEGMA does not form cylindrical or bilayered structures even at low PPEGMA compositions (<50% by weight); only spherical micelle morphologies were observed over the range of PPEGMA compositions examined (40 – 70% by weight).

2. Materials & methods

2.1. Materials

Dihydroxyl end functional poly(propylene carbonate) (PPC) (M_n = 5.6 kDa) was provided by SK Innovation [14]. Poly(ethylene glycol) methacrylate (PEGMA) (M_n = 0.5 kDa) was purchased from Aldrich. To remove free radical inhibitors, the PEGMA was purified using a column packed with 10 mL (apparent volume) of Al_2O_3 powder (≥98%, Sigma-Aldrich) and 5 mL (apparent volume) of $MgSO_4$ powder (≥99.5%, Sigma-Aldrich). 4-Cyano-4-(phenylcarbonothioylthio)pentanoic acid (CPCP, 97%, Aldrich), N,N'-dicyclohexyl carbodiimide (DCC, 99%, Aldrich), 4-(dimethylamino)pyridine (DMAP, 99%, Sigma-Aldrich), 2,2′-azobis(2-methylpropionitrile) (α,α′-azoisobutyronitrile (AIBN), 98%, Sigma-Aldrich), and dichloromethane (DCM, anhydrous 99.8%, Aldrich) were used as received. All other chemicals/solvents were purchased from Mallinckrodt Chemicals (unless noted otherwise) and used as received. Milli-Q-purified water (18 MΩ·cm^{-1} resistance) was used for all aqueous experiments.

2.2. Preparation of CPCP-PPC-CPCP

For this study, three different PPEGMA-PPC-PPEGMA block copolymer (BCP) materials (named "G7C6G7", "G3C6G3", and "G2C6G2") were prepared via reversible addition fragmentation chain transfer (RAFT) polymerization from a common, α,ω-dihydroxy functional PPC precursor (having a number-average molecular weight (M_n) of 5.6 kDa) (Fig. 1). Both ends of the PPC were functionalized with CPCP via Steglich esterification. PPC (1.16 mmol), CPCP (4.64 mmol) and DMAP (0.93 mmol) were dissolved in DCM (16.43 mL) in a round bottom flask at below 0 . DCC (4.64 mmol) was dissolved in DCM (8.22 mL) in a separate flask at below 0 . The two solutions were mixed at below 0 under nitrogen purge. The mixture was sealed and then stirred at room temperature for 24 h. Afterwards, the solution was filtered using a syringe filter (0.45 μm, PTFE, Fisher Scientific) to remove the reaction byproduct, N,N'-dibutylurea. The filtered solution was dropped into excess cold ethyl ether. The precipitate and floating material were collected by filter paper. The precipitation process was repeated two more times to remove unreacted CPCP completely. The resulting filtride was dried under vacuum and stored at 4 prior to use.

2.3. RAFT polymerization of PEGMA

PEGMA was polymerized via RAFT using CPCP-PPC-CPCP as the precursor polymer. A designated amount of PEGMA (purified with Al_2O_3/$MgSO_4$ chromatography) was mixed with 1.50 g of CPCP-PPC-CPCP in THF (20 mL); the amounts of PEGMA used were 4.43 g for G7C6G7, 1.50 g for G3C6G3, and 1.28 g for G2C6G2. 4.93 mg of AIBN was added to this reaction mixture to initiate the polymerization (AIBN:PPC = 0.1:1.0 by mole). The mixture was purged with nitrogen for 30 min and then heated to 80 under magnetic stirring. The polymerization was allowed to proceed at this temperature for 48 h. The PPEGMA-PPC-PPEGMA product was purified and collected by precipitating it in excess cold ethyl ether.

2.4. Characterization of PPEGMA-PPC-PPEGMA materials

The PPEGMA block molecular weights for the three BCPs (G7C6G7, G3C6G3, and G2C6G2) were determined by ^{1}H NMR spectroscopy. For NMR analysis, 15 mg of the polymer was dissolved in 1.0 mL of $CDCl_3$ (Cambridge Isotope Laboratories, with 0.10% v/v TMS internal reference). NMR spectra were obtained

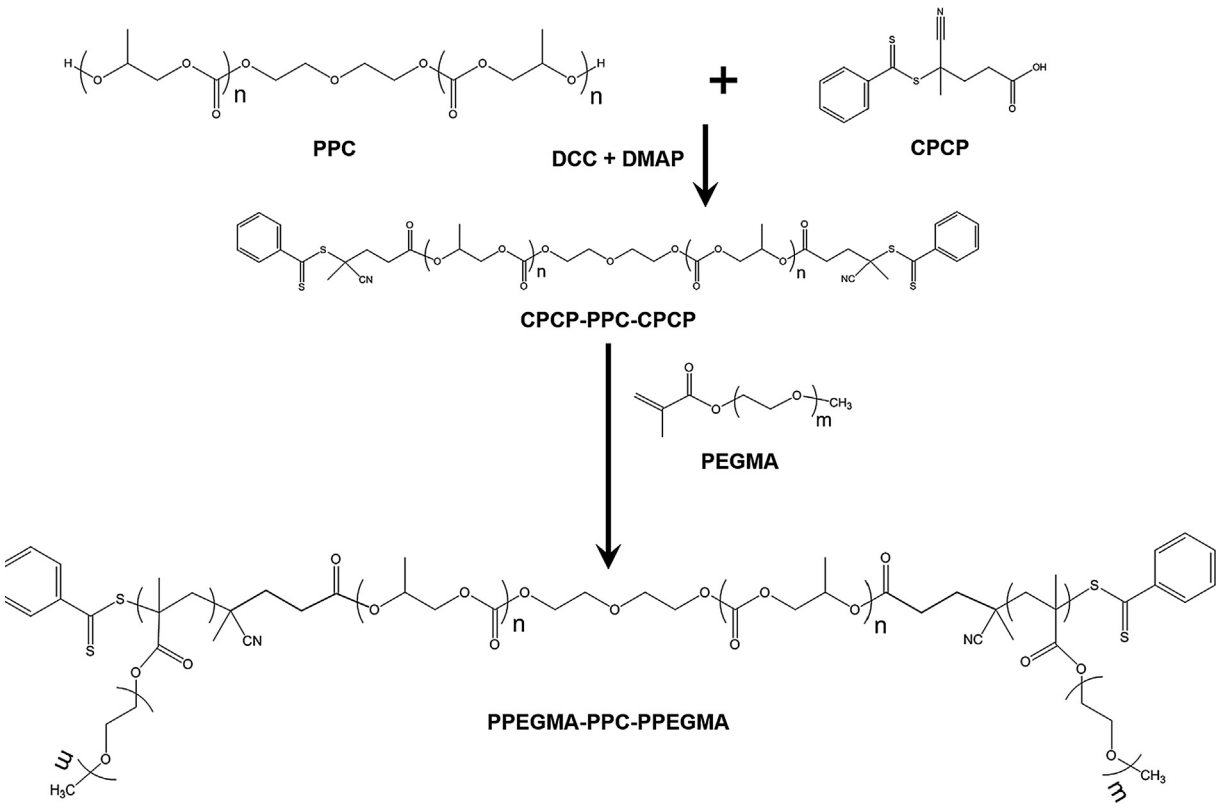

Fig. 1. General scheme for the synthesis of the poly(poly(ethylene glycol) methacrylate)-poly(propylene carbonate)-poly(poly(ethylene glycol) methacrylate)) (PPEGMA-PPC-PPEGMA) block copolymer (BCP) materials used in the present study.

using a Bruker ARX300 spectrometer operated at 300 MHz. From the NMR data (Fig. S1 of the Supporting Material (SM)), the area ratios between the peaks at ~3.4 ppm (corresponding to PPC protons labeled as "β" in Fig. S1(a)) and ~5.1 ppm (corresponding to PPEGMA protons labeled as "α" in Fig. S1(a)) were estimated to be 1.00:1.53, 1.00:0.57, and 1.00:0.46, respectively, for the G7C6G7, G3C6G3, and G2C6G2 samples, which give estimates for the overall PPEGMA block molecular weight (M_n) which are 14.5 kDa for G7C6G7, 5.2 kDa for G3C6G3, and 4.3 kDa for G2C6G2; therefore, the overall block copolymer molecular weights are estimated to be 20.1 kDa for G7C6G7, 10.8 kDa for G3C6G3, and 9.9 kDa for G2C6G2. The overall molecular weight ratios between the PPC and PPEGMA blocks are estimated to be 28:72 for G7C6G7, 52:48 for G3C6G3, and 58:42 for G2C6G2. PPEGMA is composed of a hydrophobic poly(methacrylate) (PMA) backbone, and hydrophilic short PEG side chains (0.5 kDa) (Fig. 1). Therefore, the overall PEG side chain molecular weights are estimated to be 12.5 kDa for G7C6G7, 4.5 kDa for G3C6G3, and 3.7 kDa for G2C6G2. These results are summarized in Table 1. Also, as shown in the table, the NMR analysis results indicate that all RAFT polymerization reactions proceeded to complete conversion, and the overall PPEGMA molecular weights were predominantly controlled by reaction stoichiometry.

The polydispersities of the overall molecular weight distributions of the G7C6G7, G3C6G3, and G2C6G2 materials were determined by gel permeation chromatography (GPC). For GPC analysis, 1.0 mg of the polymer was dissolved in 1.0 mL of THF. GPC traces were obtained using a Waters Breeze HPLC system equipped with two Phenogel columns (0.05 and 0.4 μm pose sizes). THF was used as the eluent at a flow rate of 0.5 mL/min at 30 ℃. GPC traces for these polymers are presented in Fig. S2. The polydispersity indices (PDIs) are estimated to be 1.30 for G7C6G7, 1.28 for G3C6G3, and 1.37 for G2C6G2 (Table 1). As shown in Fig. S2 of the SM, all samples exhibited monodisperse peaks, suggesting that there is no unreacted PPC precursors remaining or erroneously produced PPEGMA homopolymers (polymerized from non-PPC-attached RAFT agents).

2.5. Preparation & characterization of PPEGMA-PPC-PPEGMA micelles

0.3 g of dried PPEGMA-PPC-PPEGMA (G7C6G7, G3C6G3 or G2C6G2) was placed in 14.7 g of Milli-Q water. The solution was stirred using a magnetic stirrer for 24 h. Typically, the polymer was completely visually dissolved in water within 24 h. The hydrodynamic sizes of PPEGMA-PPC-PPEGMA micelles in deionized water were measured by DLS using a ZetaPALS instrument (Brookhaven Instruments). For DLS measurements, 0.03 wt% polymer solutions were used to avoid multiple scattering effects. The polymer micelles were directly visualized by cryo-TEM using a 300 kV FEI Titan Krios electron microscope. TEM specimens were prepared as follows. A formvar/carbon-coated TEM grid (Ted Pella) was plasma cleaned for 30 s in a Solarus system (Gatan). The cleaned grid was placed in a controlled environmental chamber, in which the atmosphere was humidified to near saturation (to prevent evaporation of water from the solution sample). Inside this chamber, a 3–4 μL droplet of the micelle solution was placed on the grid, and excess liquid was removed by soaking with filter paper. The solution remaining inside the grid was vitrified by plunging the whole grid into liquid ethane. Appropriate phase contrast was generated at a nominal underfocus of about 5–10 μm. The raw images were background subtracted and normalized using Gatan's Digital Micrograph software. Steady shear measurements were performed using a DHR-2 stress-controlled rheometer (TA Instruments) equipped with a Peltier Couette cell composed of a 30.37-mm-diameter cup and a 27.98-mm-diameter 42.00-mm-length bob. About 20 mL of the micelle solution was loaded in the gap between the concentric cylinders, and the Peltier temperature was set at 25 . Measurements were performed during a steady rate sweep from low to high shear rates (0.158–1000 1/s) in logarithmic intervals. The viscosity sampling period was 100 s. At each shear rate, steady state was defined as variations in viscosity <5% in three consecutive measurements. The maximum equilibration time was set at 5000 s.

2.6. Measurement of surface pressure-area isotherms

The surface pressure-area isotherms of Langmuir PPEGMA-PPC-PPEGMA monolayers were measured using a KSV 5000 Langmuir trough (58.0 cm × 15.0 cm × 0.9 cm) with a subphase volume of 1,172 mL. Double symmetric Teflon barriers were positioned at each side of the trough and moved at a constant rate of 3 mm/min for compression of the monolayer. A platinum Wilhemly plate was used to measure the surface tension of a PPEGMA-PPC-PPEGMA monolayer, which was flame-cleaned and gently washed with deionized water before use. The trough and barriers were cleaned with ethanol and deionized water trice before measurement. After filling the trough with deionized water, the water surface was aspirated to remove any dust. The cleanliness of the water surface was confirmed by the constancy of the water surface tension (within less than ±0.5 mN/m) during a blank compression. Afterward, the surface pressure was zeroed. 1.0 or 5.0 mg of PPEGMA-PPC-PPEGMA was dissolved in 1.0 mL of chloroform at least 24 h before spreading. A designated amount of the polymer solution was spread on the water surface by placing droplets at uniformly spaced locations on the water surface using a Hamilton micro syringe; the exact values of polymer concentration and spreading volume used are presented in Table S1 of the SM. Complete evaporation of chloroform was confirmed by monitoring the surface pressure without compression. The constant-compression surface pressure-area isotherm measurement was started after the surface pressure reached a constant value under no compression.

3. Results & discussion

3.1. Sizes of PPEGMA-PPC-PPEGMA micelles

For this study, three different PPE**G**MA-PP**C**-PPE**G**MA BCP materials having an identical PPC molecular weight (**5.6** kDa) and

Table 1
Molecular characteristics (block molecular weights and overall polydispersity indices) of the PPEGMA-PPC-PPEGMA BCP materials used in the present study. † Determined by NMR. ‡ Determined by GPC.

Sample	PPC:PPEGMA weight ratio		PPC M_n (kDa)	PPEGMA M_n (kDa)			PPEGMA-PPC-PPEGMA	
	Target	Actual		PMA	PEG	PPEGMA	M_n (kDa)	PDI
$PPEGMA_{7.2K}$-$PPC_{5.6K}$-$PPEGMA_{7.2K}$ (G7C6G7)	30:70	28:72	5.6†	2.0†	12.5†	14.5†	20.1† (21.5‡)	1.30‡
$PPEGMA_{2.6K}$-$PPC_{5.6K}$-$PPEGMA_{2.6K}$ (G3C6G3)	50:50	52:48	5.6†	0.7†	4.5†	5.2†	10.8† (13.7‡)	1.28‡
$PPEGMA_{2.1K}$-$PPC_{5.6K}$-$PPEGMA_{2.1K}$ (G2C6G2)	60:40	58:42	5.6†	0.6†	3.7†	4.3†	9.9† (11.3‡)	1.37‡

different PPEGMA molecular weights (**7.2**, **2.8** and **2.1** kDa on either side) (named "**G7C6G7**", "**G3C5G3**", and "**G2C6G2**", respectively) were prepared (Fig. 1). The molecular weight characteristics of these polymers are summarized in Table 1. Micellar solutions of the G7C6G7, G3C6G3 and G2C6G2 polymers (0.03 wt%) were prepared by simple hydration of dried polymer in deionized water. The hydration processes were monitored by DLS. As shown in Fig. 2, the sizes of G7C6G7 and G2C6G2 micelles reached their final values within less than a few days (i.e., within about 1 and 3 days, respectively), whereas it took about two weeks (~13 days) for G3C6G3 micelles to reach (apparent) equilibrium. Notably, the final hydrodynamic radii of the G7C6G7, G3C6G3 and G2C6G2 micelles were determined to be 15.4 ± 1.4 nm (averaged from t = 1 to 30 days post hydration), 30.9 ± 0.7 nm (averaged from t = 13 to 30 days post hydration) and 804 ± 142 nm (averaged from t = 3 to 30 days post hydration), respectively. In the literature, it has been reported that block copolymer micelle sizes typically increase with decreasing length of the hydrophilic block, if the hydrophobic block length is fixed, because of the transformation of the micelle shape from spheres to larger aggregates (such as cylinders and vesicles) [7,8]. Therefore, the results displayed in Fig. 2 are seemingly consistent with this previously reported trend in that, as we go from G7C6G7 to G3C6G3 to G2C6G2, the hydrophilic composition of the copolymer decreases (w_{PPEGMA} (overall PPEGMA weight fraction) = 0.72, 0.48 and 0.42 for G7C6G7, G3C6G3 and G2C6G2, respectively, and w_{PEG}(overall PEG weight fraction) = 0.62, 0.41 and 0.37 for G7C6G7, G3C6G3 and G7C6G7, respectively). In order to validate the size trend observed in the DLS data, aqueous micellar solutions of G7C6G7, G3C6G3 and G2C6G2 (2.0 wt%) were also visually inspected. The series of photographs presented in Fig. S3 indeed support the formation of large aggregates in the aqueous G2C6G2 solution, which renders the solution completely turbid, whereas the G7C6G7 solution is optically transparent (G7C6G7 micelles are small enough not to strongly scatter visible light). G3C6G3 in behavior is intermediate between G7C6G7 and G2C6G2; the G3C6G3 solution is translucent (Fig. S3).

3.2. Langmuir monolayers of PPEGMA-PPC-PPEGMA

An important feature that distinguishes PPEGMA-PPC-PPEGMA from more commonly studied, linear PEG-based amphiphilic block copolymers (such as poly(butadiene)-PEG [7,8]) is the branched

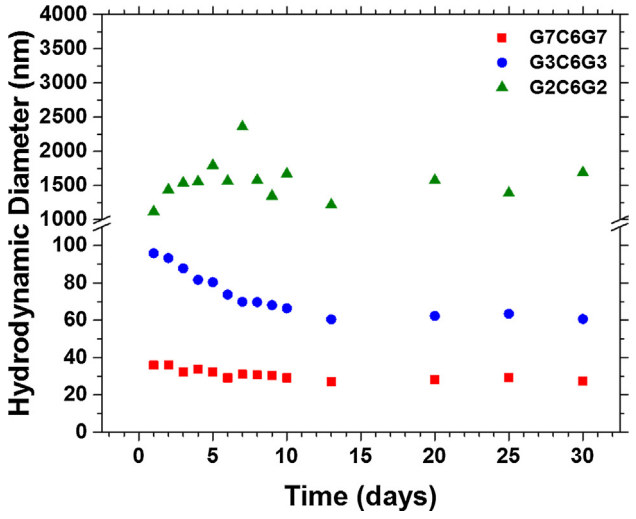

Fig. 2. Mean hydrodynamic diameters of G7C6G7, G3C6G3 and G2C6G2 micelles (0.03 wt%) in water.

architecture of the PPEGMA segment; multiple short (500 Da) hydrophilic PEG side chains are attached to a hydrophobic PMA backbone chain. Therefore, an important question that arises is: When PPEGMA-PPC-PPEGMA chains form micelles, which portions of the PPEGMA-PPC-PPEGMA chain exist in the hydrated state? (In other words, is it the entire PPEGMA block, or only the PEG side chains, that become(s) hydrated?) In order to answer this question, the molecular conformational characteristics of the G7C6G7, G3C6G3 and G7C6G7 polymers were first examined under more controlled environmental conditions, i.e., using the air–water interface as a mimic for the hydrophobic core-aqueous interface of the micelles; surface pressure-area isotherm measurements were performed on Langmuir monolayers formed at the air–water interface by these G7C6G7, G3C6G3 and G7C6G7 polymers. The results are presented in Fig. 3(a) through (c). As shown in the figures, all isotherms exhibited common general features. Most notably, the isotherm curves show two surface pressure plateaus, one at around 15 mN/m surface pressure, and the other at surface pressures near/above 25 mN/m. These features were most clearly visible in the G7C6G7 data (Fig. 3(a)) because of its longest PPEGMA block length. To understand the origin of this behavior, additional isotherm measurements were also performed on Langmuir monolayers of PPC (M_n = 5.6 kDa, DP_n = 55) and PPEGMA (M_n = 13.2 kDa, DP_n = 26) homopolymers (Fig. 3(d) and 3(e), respectively). As shown in Fig. 3(d), the PPC homopolymer itself exhibits a surface pressure plateau at monolayer collapse around ~15 mN/m during compression in the range of monolayer area between about 510 and 120 Å^2 per chain (i.e., between about 9.3 and 2.2 Å^2 per PPC monomer). At surface areas less than about 2.2 Å^2 per monomer, the PPC isotherm shows a steep rise in surface pressure in response to compression because of the glassy nature of the PPC material at room temperature ($T_g \approx 35$ °C for bulk PPC [15]); the compression rate dependence of the PPC isotherm presented in Fig. S7(b) further supports this interpretation, as discussed in detail in Ref. [16]. The overall behavior of PPC is quite similar to that of glassy PLGA ($T_g \approx$ 45 °C [17]) [16,18]. As shown in Fig. 3(e), the PPEGMA isotherm also shows a plateau at ~12 mN/m due to the submergence of the PEG segments, similarly to what happens with linear PEG chains at the air–water interface [19].

The above results obtained with PPC and PPEGMA homopolymers (Fig. 3(d) and 3(e), respectively) and also previous results obtained with other polymers (such as poly(lactic-*co*-glycolic acid)-poly(ethylene glycol) (PLGA-PEG) [20] and poly(*n*-butyl acrylate)-poly(ethylene glycol) (PnBA-PEG) [21]) enable us to deduce the following explanations for the occurrence of the two distinct plateaus in the compression isotherms of the PPEGMA-PPC-PPEGMA monolayers (Fig. 3(a) through 3(c)). Firstly, the initial plateau at a surface pressure of ~15 mN/m occurs due to the surface-adsorbed-to-submerged transition of the PEG side chains, which is reminiscent of the behavior of the PPEGMA homopolymer shown in Fig. 3(e). The second plateau occurring at a surface pressure near or slightly above 25 mN/m, on the other hand, does not appear to be associated with the formation and collapse of a water-free monolayer of the PPC middle block polymer for the following two reasons. First, the plateau pressure is too high ($\gtrsim$ 25 mN/m) to be assigned to a collapse transition in a PPC monolayer (~15 mN/m, Fig. 3(d)). Second, the surface area per chain values at the onset of the second surface pressure plateau are not constant among the three PPEGMA-PPC-PPEGMA triblock materials studied (Fig. 3(a) through 3(c)) (even though the three triblock copolymers have the same PPC block length); the area per chain values at the onset of the second plateau are estimated to be 500 Å^2 per chain (9.1 Å^2 per PPC monomer) for G7C6G7 (Fig. 3(a)), 200 Å^2 per chain (3.6 Å^2 per PPC monomer) for G3C6G3 (Fig. 3(b)), and 170 Å^2 per chain (3.1 Å^2 per PPC monomer) for G2C6G2 (Fig. 3(c)). Note that for

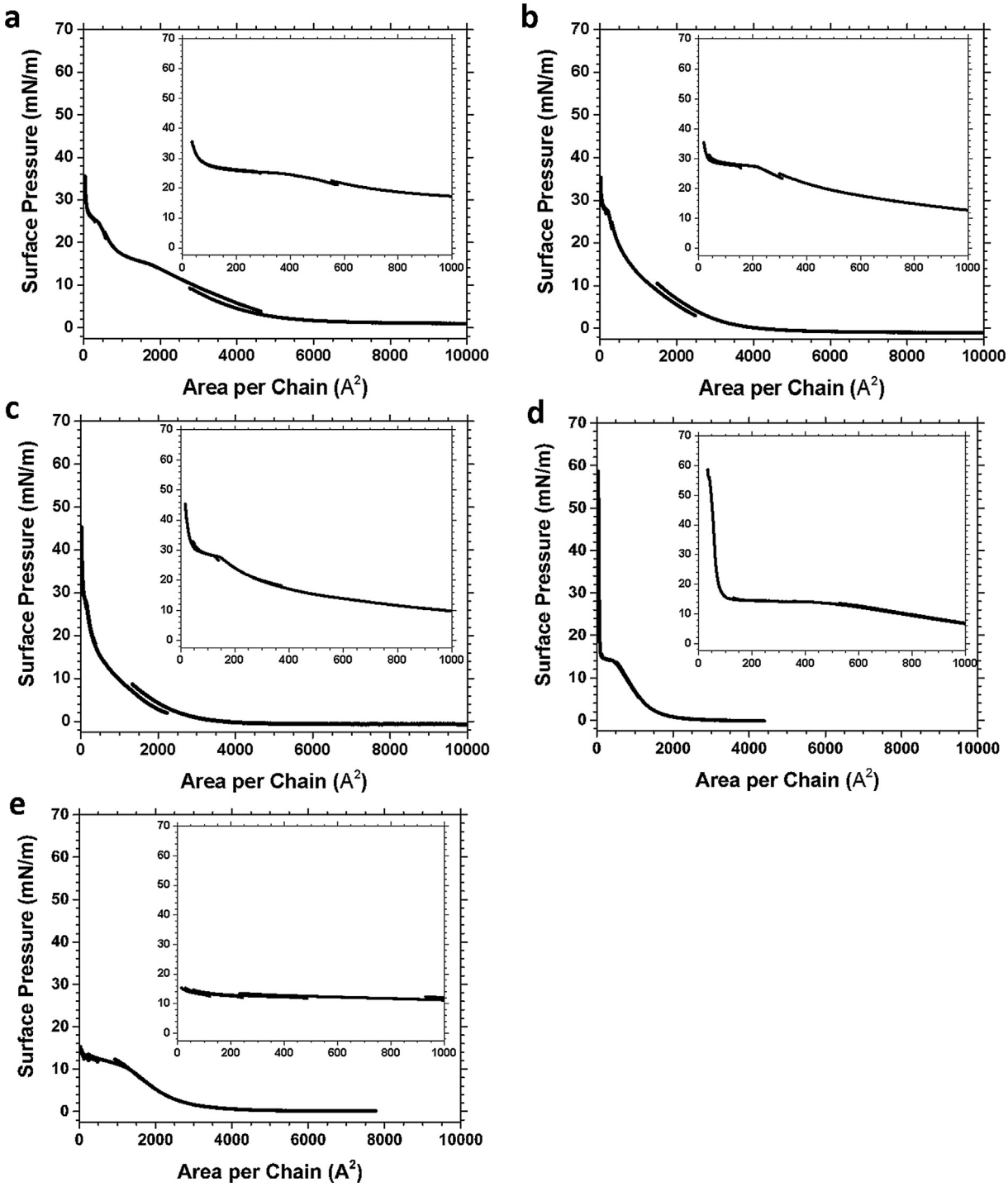

Fig. 3. Constant compression rate (3 mm/min) surface pressure-area isotherms for chloroform-spread **(a)** G7C6G7 (M_n = 20.1 kDa, PPC:PPEGMA = 28:72 by weight), **(b)** G3C6G3 (M_n = 10.8 kDa, PPC:PPEGMA = 52:48 by weight), **(c)** G2C6G2 (M_n = 9.9 kDa, PPC:PPEGMA = 58:42 by weight), **(d)** PPC (M_n = 5.6 kDa), and **(e)** PPEGMA (M_n = 13.2 kDa) at the air–water interface at 25 °C. Data are redrawn in Fig. S4 in plots of surface pressure vs. concentration.

the PPC precursor the onset occurs at 510 Å^2 per chain or 9.3 Å^2 per PPC monomer (Fig. 3(d)).

A more plausible explanation is that the second plateau is caused by the formation of a continuous water-free monolayer by the PMA backbone chains of the PPEGMA blocks. This explanation is supported by the fact that the values of surface area per PMA monomer at the onset of the plateau are constant independent of the length of the PMA backbone; the plateau onset areas are estimated to be 22.8 Å^2 per PMA monomer for G7C6G7 (Fig. 3(a)), 22.4 Å^2 per PMA monomer for G3C6G3 (Fig. 3(b)), and 23.2 Å^2 per PMA monomer for G2C6G2 (Fig. 3(c)). These results are also consistent with literature data on similar methacrylate-based polymers; poly(*n*-propyl methacrylate) (PnPMA), for instance, has been shown to collapse at about 21 Å^2 per monomer (at ~20 mN/m) [17]. We speculate that the PPC blocks become expelled from the interface relatively early during the compression process, i.e., while the PMA backbone chains are still continuously being concentrated at the interface, which causes the PPC collapse

process to be undetectable by surface pressure measurement. It should also be noted that the PMA backbone becomes fully anchored to the air–water interface only in the PPEGMA-PPC-PPEGMA situation; the Langmuir isotherm of the PPEGMA homopolymer does not show a secondary plateau (Fig. 3(e)). The abrupt increase in surface pressure observed at highest compression level examined (Fig. 3) is linked to the glass transition of the collapsed PPC film formed on the air-side of the PMA monolayer; the data in Figs. S6 and S7(a) also support this view.

One might question whether the plateaus in the surface pressure-area isotherms could be caused by the desorption of the polymers from the air–water interface into the subphase. It is well documented that Langmuir monolayers (i.e., "spread" monolayers) formed by water-soluble polymers (such as PEG) typically do not show any additional increase in surface pressure following a plateau during compression even at high polymer concentrations [19]; of note, this behavior should not be confused with that of Gibbs monolayers (i.e., "adsorbed" monolayers) of water-soluble polymers (e.g., PEG), which often exhibit an upturn of surface pressure under high compression, when the subphase solution is fully saturated with the dissolved polymers [22]. Therefore, the rapid increase in surface pressure under high compression observed with Langmuir PPEGMA-PPC-PPEGMA monolayers suggests that the surface pressure plateau is not caused by the desorption of the polymers into the subphase, and also that the PPEGMA-PPC-PPEGMA polymers are not, in fact, molecularly soluble in water (thus these polymers likely have zero CMC, and their micelles can be considered as type "2" micelles defined in the Introduction).

Lastly, it should be noted out that all above explanations (i.e., the surface pressure plateau at ~15 mN/m surface pressure due to the submergence of the PEG chains, and the second plateau near/above 25 mN/m due to the formation and collapse of PMA monolayers) are also consistent with the fact that the plateau features are most conspicuous with G7C6G7 (which has the largest PPEGMA block length); within our picture the widths of the plateaus in the surface pressure-area curve are expected to be linearly proportional to the size of the PPEGMA block. Taken together, these results suggest that when PPEGMA-PPC-PPEGMA chains form Langmuir films, only the PEG side chains are hydrated, and the hydrophobic PMA backbone is situated between the aqueous phase and the hydrophobic domain formed by the PPC chains; see Fig. 4 for schematic depiction of this concept.

3.3. Morphological and conformational properties of PPEGMA-PPC-PPEGMA micelles

The PPEGMA-PPC-PPEGMA micelles were directly visualized by cryogenic transmission electron microscopy (cryo-TEM). Representative cryo-TEM images are presented in Fig. 5. Interestingly, it was found that changes of PPEGMA block length do not cause any changes in basic micelle shape; all three PPEGMA-PPC-PPEGMA materials studied (G7C6G7 (w_{PPEGMA} = 0.72), G3C6G3 (w_{PPEGMA} = 0.48), and G2C6G2 (w_{PPEGMA} = 0.42)) form spherical micelles (Fig. 5). However, as also can be seen from Fig. 5, there appears to exist differences among the three samples in the way the micelles are dispersed in solution. Particularly, the behaviors are noticeably different between the G7C6G7 and G2C6G2 systems; G7C6G7 micelles are dispersed as isolated micelles, whereas G2C6G2 micelles appear to form large clusters. The behavior of G3C6G3 appears to be intermediate; the G3C6G3 micelles appear to be able to form only small clusters (e.g., dimers, trimers, etc.), although cryo-TEM images cannot be used as definitive evidence for such a conclusion because of flow-induced artifacts associated with sample preparation for cryo-TEM studies [23]. These observations are, however, quite consistent with the DLS data presented in Fig. 2 and also with the visual observation of transparency/opacity of the solutions discussed earlier with reference to Fig. S3.

These cryo-TEM results raise two important questions. First, what causes PPEGMA-PPC-PPEGMA micelles to cluster? Second, why do only PPEGMA-PPC-PPEGMA micelles with relatively short PPEGMA chains (G2C6G2 micelles) form clusters while PPEGMA-PPC-PPEGMA micelles with long PPEGMA chains (G7C6G7 micelles) do not cluster? As will be discussed in detail later, we believe that the micelle clusters are formed because of the insufficient coverage of the micelle core surface by PEG chains under certain circumstances. In order to understand why G2C6G2 micelles predominantly exist in clusters, whereas G7C6G7 micelles prefer to remain dispersed as isolated micelles in water, the structural characteristics of the micelle core domains visualized in the cryo-TEM studies were further analyzed quantitatively; assuming that both the PPC middle block and PMA backbone segments constitute the core domain of the micelle (as suggested by the surface pressure-area isotherms (Fig. 3)), the grafting densities of the PEG chains on the micelle core surfaces were calculated. The results are summarized in Table 2. As shown in the table, evaluated PEG grafting densities were found to be significantly different between the G7C6G7 and G2C6G2 systems; G7C6G7 micelles have a much denser PEG brush layer (i.e., $\sigma_{PEG} \times \pi R_{g,PEG}^2$ (dimensionless PEG grafting density) ≈ 16.8; see the table caption for the definitions of the notations) than G2C6G2 micelles ($\sigma_{PEG} \times \pi R_{g,PEG}^2 \approx$ 6.55). The sparser surface coverage of PEG chains on G2C6G2 micelles allows a closer approach between a pair of micelles, which may (i) result in the formation of inter-micellar PEG bridges and/or (ii) cause the van der Waals attraction between the micelle cores to become non-negligible (Fig. 5(e)). The dense PEG brush layer in the case of G7C6G7 provides steric hindrance preventing micelles from approaching closely and hence preventing any of these effects (Fig. 5(d)).

3.4. Calculation of the attractive forces between PPEGMA-PPC-PPEGMA Micelles: Bridging vs. Van der Waals interactions

In order to first examine the reasonableness of the PEG bridging hypothesis, we performed a simple thermodynamic analysis as follows. The analysis starts with the assumption that PEG bridging is caused by the hydrophobic effect; the PEG side chains have methoxy end groups (–OCH_3). It is known that the free energy change associated with transferring the methyl end group (of a hydrocarbon chain) out of water and into the micelle's hydrophobic interior is $\Delta g \approx -1.59 \times 10^{-20}$ J (=−9.60 kJ/mol) [24]; note the room temperature thermal energy (k_BT) is about 4.12×10^{-21} J (=2.48 kJ/mol). We assume that this Δg information is applicable to the methoxy PEG situation. Stable binding between two micelles would require the inter-micellar binding free energy (ΔG) to be greater in magnitude (more negative) than ~−5 k_BT (a condition for phase separation in colloids [25]). Therefore, in order to form stable micelle clusters, only a couple of PEG bridges would need to be formed between two adjacent micelles. From the cryo-TEM image in Fig. 5(c), it is possible to estimate the (maximum likely) number of bridging strands between two G2C6G2 micelles. From Fig. 5(c), the mean closest core surface-to-surface separation distance between two adjacent micelles (D) is estimated to be about 3.70 nm. The fully stretched contour length of the PEG side chain (L) is about 5.10 nm ($DP_{n,PEG} \approx 11.4$, $l_{EG} \approx 4.47$ Å (monomer length) [26]). Therefore, as schematically explained in Fig. 6(b), inter-micellar PEG bridges can only be formed in the region of the micelle gap in which the surface-to-surface distance is less than the fully stretched PEG length (L ≈ 5.10 nm). The micelle surface area within this bridging zone (A) can be calculated using the following formulas

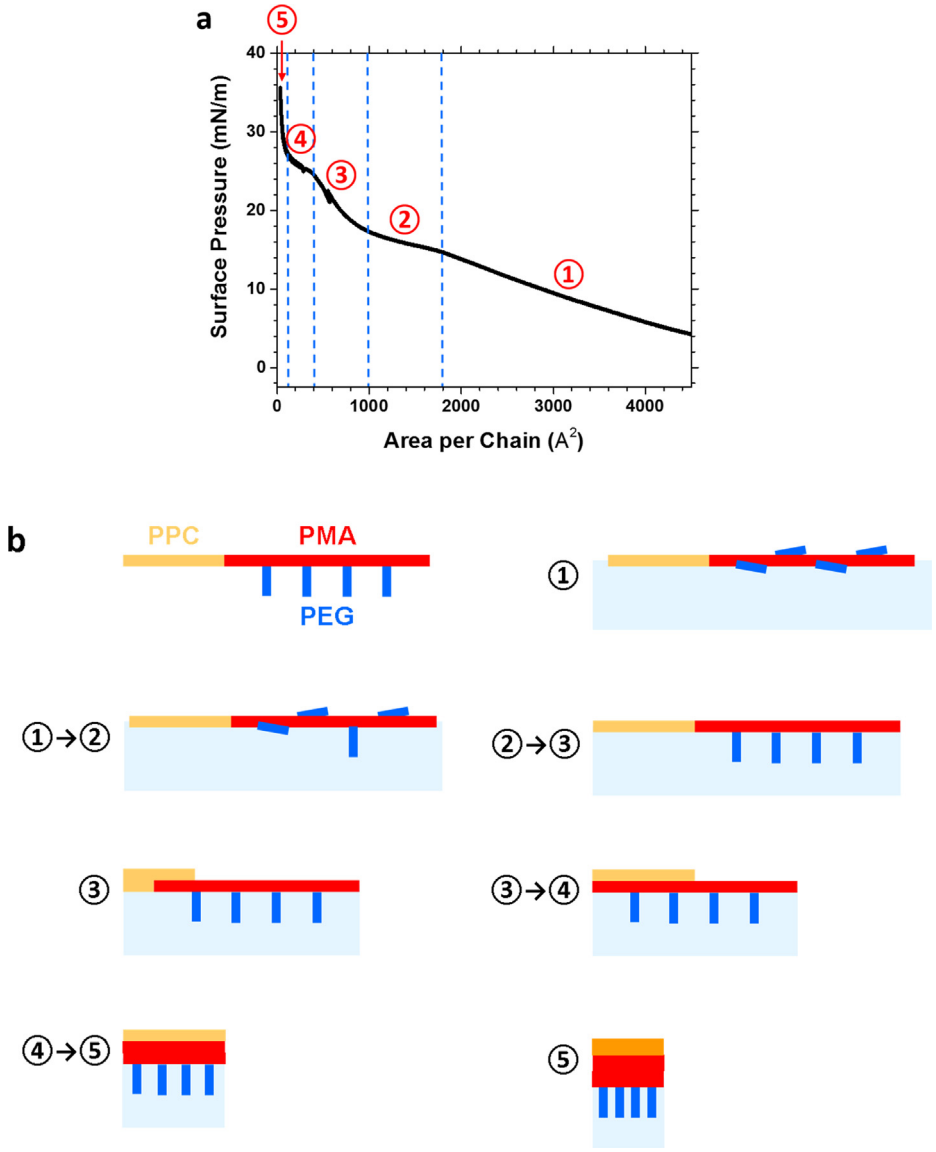

Fig. 4. Schematic depiction of conformational changes that are thought to occur in PPEGMA-PPC-PPEGMA chains at the air–water interface during compression. **(a)** The surface pressure-area isotherm for G7C6G7 (M_n = 20.1 kDa, PPC:PPEGMA = 28:72 by weight) redrawn from Fig. 3(a). In PPEGMA-PPC-PPEGMA cartoons, only the half of the polymer structure is shown for simplicity. **(b)** ①: PPEGMA-PPC-PPEGMA chains lie flat on the water surface. ①→②: PEG side chains start submerging into the subphase. ②→③: All PEG side chains become fully submerged into the subphase. ③: PPC segments are increasingly collapsed into multilayers. ③→④: Water surface becomes fully covered by a continuous monolayer of PMA. ④→⑤: Collapsed glassy domains formed by PPC chains start becoming interconnected into a space-spanning structure. ⑤: The Langmuir PPEGMA-PPC-PPEGMA film is mechanically resistant to lateral compression.

$$A = 2\pi R_c^2 \int_0^{\theta} \sin\theta' d\theta' \quad (1)$$

$$\theta = \sin^{-1}\left(\frac{Y}{R_c}\right) \quad (2)$$

$$Y \approx (2R_cX)^{1/2} \text{ (Chord Theorem)} \quad (3)$$

$$X = \frac{L}{2} - \frac{D}{2} \quad (4)$$

where R_c is the micelle core radius (≈ 12.7 nm for G2C6G2 micelles, determined from Fig. 5(c) via ImageJ analysis, Table 2), and other notations (θ, X, and Y) are defined in Fig. 6(a). We estimate A ≈ 57.5 nm^2 at D = 3.7 nm, and accordingly the maximum number of PEG bridges that can be formed between adjacent G2C6G2 micelles is estimated to be $N_{b,1}$ (=$2\sigma_{PEG}A$) ≈ 504; here, the factor, 2, is introduced because of the mutual interdigitation of the PEG chains from each micelle. The inter-micellar binding free energy can therefore be estimated; ΔG (=$N_{b,1}\Delta g$) ≈ -8.04×10^{-18} J = -1.95×10^3 k_BT, which would indeed provide a sufficient driving force for the formation of clusters. The above model in fact enables us to further estimate ΔG as a function of D in the range 3.7–5.1 nm (Fig. 7(a)); as shown in Fig. 7(a), ΔG was found to vary linearly with D. The slope of this ΔG vs. D curve gives an estimate of the force required to break apart the inter-micelle bonds, F_1 = dΔG/dD. For G2C6G2 micelles, this breakup force is estimated to be $F_1 \approx 5.75 \times 10^{-9}$N. As will be discussed in detail later, this result suggests that these micelle clusters would be difficult to break apart completely using ordinary methods of mechanical agitation or shear. In fact, it is more reasonable to expect that the magnitude of the anchoring free energy of the methoxy end group ($-OCH_3$) of the PEG side chain is significantly smaller than that of the methyl end group ($-CH_2CH_3$) of a hydrocarbon chain (|Δg

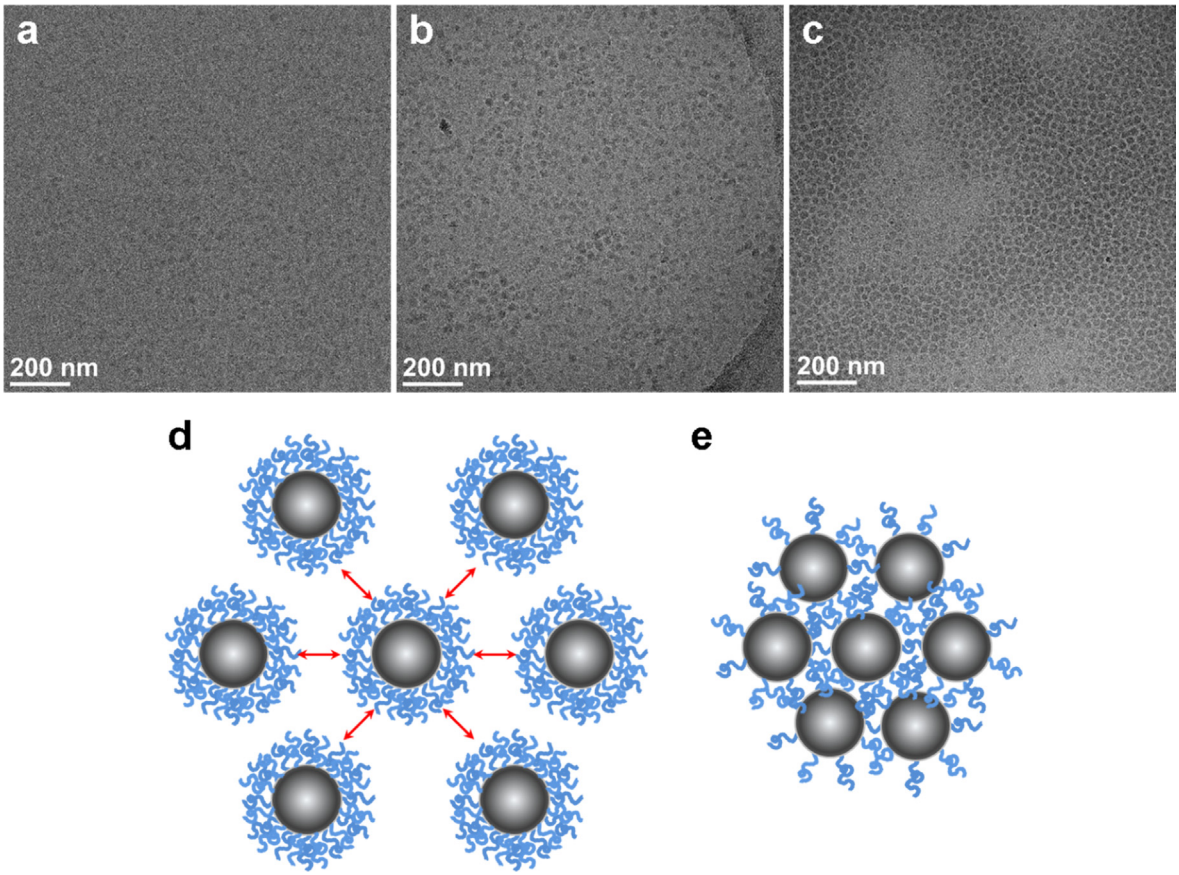

Fig. 5. **(Top)** Cryo TEM images of 0.5 wt% **(a)** G7C6G7 (M_n = 20.1 kDa, PPC:PPEGMA = 28:72 by weight), **(b)** G3C6G3 (M_n = 10.8 kDa, PPC:PPEGMA = 52:48 by weight), and **(c)** G2C6G2 (M_n = 9.9 kDa, PPC:PPEGMA = 58:42 by weight) solutions in water. **(Bottom)** Cartoons describing the agglomeration states of **(d)** G7C6G7 micelles, and **(e)** G2C6G2 (and G3C6G3) micelles in water. G7C6G7 micelles are repulsive to each other and exist predominantly as isolated micelles because of their densely grafted PEG brush chains that produce steric effects. G2C6G2 (and G3C6G3) micelles are weakly attracted to each other and form clusters, because the relatively low PEG grafting density allows the micelles to approach one another closely so that the van der Waals interaction becomes important.

Table 2
Hydrodynamic radii of micelle agglomerates (R_h, estimated by viscometry (at $\dot{\gamma}$ = 0.159 s^{-1}) and DLS), and micelle core radii (R_c, estimated by cryo-TEM). A_c = micelle core surface area (=$4\pi R_c^2$). V_c = micelle core volume (=$4\pi R_c^3/3$). v_{PPC} = molecular volume of the PPC block (estimated assuming a density of 1.26 g/cm^3 for PPC). v_{PMA} = overall molecular volume of the two PMA backbones per PPEGMA-PPC-PPEGMA chain (estimated assuming a density of 1.18 g/cm^3 for PMA). N_{agg} = number of PPEGMA-PPC-PPEGMA chains per micelle (=$V_c/(v_{PPC} + v_{PMA})$). N_{PEG} = number of PEG side chains per micelle (=$N_{agg} \times (M_{n,PEG}/m_{PEG})$, where $M_{n,PEG}$ = total molecular weight of PEG side chains per PPEGMA-PPC-PPEGMA chain (6th column in Table 1), and m_{PEG} = PEG side chain molecular weight (=500 g/mol)). σ_{PEG} = grafting density of the PEG side chains (=N_{PEG}/A_c). $R_{g,PEG}$ = radius of gyration of the PEG side chain in the three-dimensional self-avoiding random-walk configuration (estimated using parameters from Ref. [33]).

Sample	$R_{h,DLS}$ (nm)	$R_{h,vis}$ (nm)	$R_{c,TEM}$ (nm)	$A_c \times 10^3$ (nm^2)	$V_c \times 10^3$ (nm^3)	$v_{PPC} + v_{PMA}$ (nm^3)	N_{agg}	$N_{PEG} \times 10^3$	σ_{PEG} (nm^{-2})	$\sigma_{PEG} \times \pi R_{g,PEG}^2$
G7C6G7	15.4	34.4	11.9	1.78	7.06	10.2	693	17.3	9.71	16.8
G3C6G3	30.9	395	12.1	1.84	7.42	8.38	885	7.89	4.29	7.43
G2C6G2	804	16,872	12.7	2.03	8.58	8.21	1046	7.66	3.78	6.55

$(-CH_2CH_3)$ | ≈ 3.86 k_BT); it is more likely that $|\Delta g(-OCH_3)| \ll k_BT$, and thus the PEG chain end anchoring is unlikely to occur (as will be discussed again later).

The van der Waals potential energy of attraction between two spherical micelle cores can be estimated by [24]

$$U \approx -\frac{H_{121}R_c}{12D} \quad (\text{for } D \ll R_c) \tag{5}$$

where H_{121} is the Hamaker constant; the subscript, 121, indicates two spheres made of material 1 (PPC + PMA) separated by a medium of material 2 (water). Using the values, $H_{121} = 1.05 \times 10^{-20}$ J (for poly(methyl methacrylate) in water [24] as an approximation) and R_c = 12.7 nm (determined by cryo-TEM, Table 2), the values of U were calculated as a function of D. The results are displayed in Fig. 7(b). From the U vs. D curve, the force needed to separate two clustered G2C6G2 micelles from each other is estimated to be $F_1 = dU/dD|_{D\approx 3.7nm} \approx 4.69 \times 10^{-13}$N, which is about four order of magnitude smaller than that estimated for the PEG bridging flocculation above. We note that a more accurate estimation of the inter-micelle potential energy would require an analysis of the steric interactions between the micelles caused by the PEG brush chains. However, the small size of the PEG side chains ($DP_{n,PEG} \approx 11.4$) makes it inappropriate to use simple models (such as that of de Gennes [27]) for this analysis. Nevertheless, we can predict that the actual breakup force would be smaller than what is predicted solely based on the van der Waals contributions ($F_1 \approx 4.69 \times 10^{-13}$N), because the steric effects only give rise to a repulsive contribution to the interaction potential.

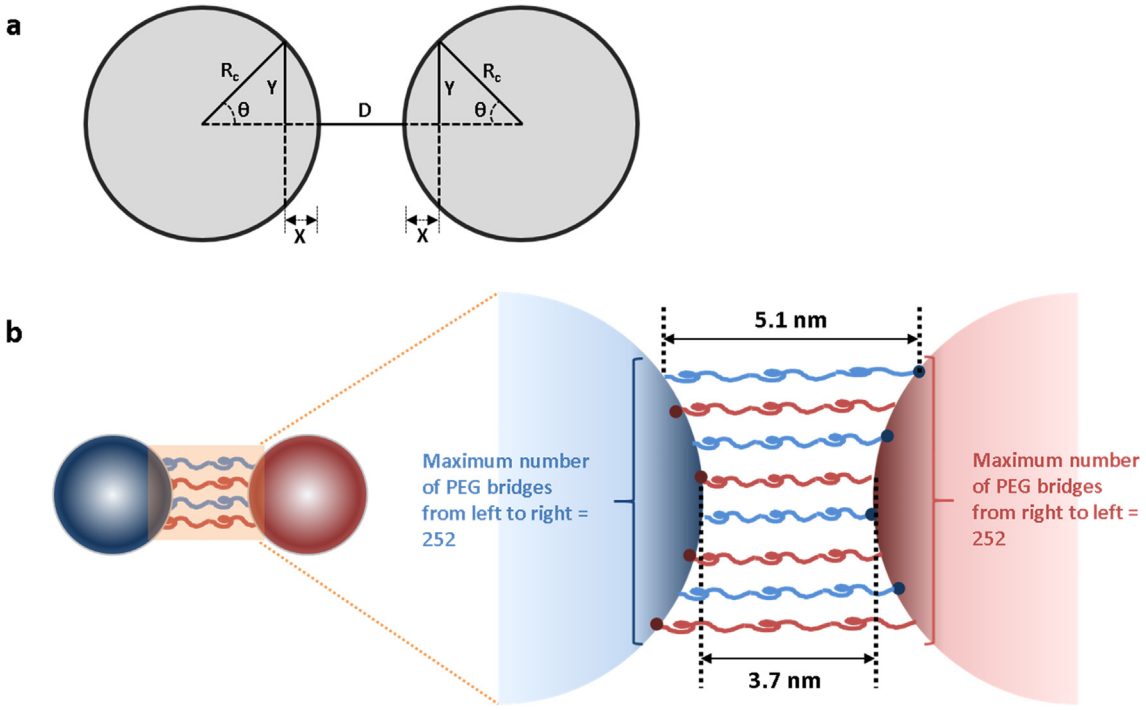

Fig. 6. **(a)** Definitions of the parameters and variables used for the calculation of the G2C6G2 micelle dimer breaking force. D is the closest inter-micellar core surface-to-surface distance. R_c is the core radius of the G2C6G2 micelles. θ is the polar angle defining the boundary of the region in which the inter-micellar surface distance is less than the fully stretched length of the PEG brush chain (≈ 5.1 nm) when D ≈ 3.7 nm (as determined by cryo-TEM). X and Y are distances as shown in the figure. **(b)** Cartoon demonstrating the conformations of PEG chains that form inter-micellar bridges.

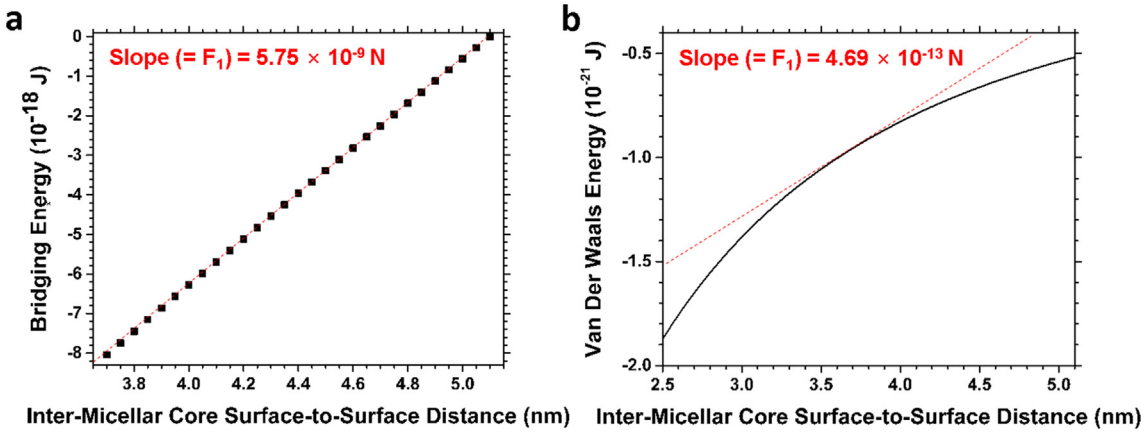

Fig. 7. Binding free energy between two adjacent G2C6G2 micelles as a function of inter-micellar core surface-to-surface distance. It is assumed that micelle binding occurs due to **(a)** the formation of inter-micellar PEG bridges or **(b)** the van der Waals forces. The slope of the line at the measured inter-micelle distance of 3.7 nm corresponds to the magnitude of the micelle dimer breaking force.

3.5. Rheological characterization of PPEGMA-PPC-PPEGMA micelle solutions

To experimentally test these predictions, we performed steady shear viscosity measurements using a Couette rheometer. Fig. 8 displays the results. As shown in the figure, a G2C6G2 micelle solution exhibits shear thinning with a power-law exponent of −0.37 over the shear rate range of $\dot{\gamma} \approx 1$ – 100 s^{-1} ($\eta \sim \dot{\gamma}^{-0.37}$), whereas G3C6G3 and G7C6G7 micelle solutions exhibit Newtonian behavior with constant viscosities over that same range of shear rates ($\eta \approx 1.21 \times 10^{-3}$ and 0.914×10^{-3} Pa·s, respectively). Note that at shear rates higher than 100 s^{-1}, all three samples show apparent increase in viscosity with increasing shear rate, which is a measurement artifact caused by non-laminar (periodic/turbulent) flows that develop in the high shear regime [28]; at >100$\dot{\gamma}$ s^{-1}, the Reynolds number, $\mathrm{Re} \equiv R^2\Omega\rho/\eta$ (R and Ω are the radius and angular velocity of the rotating bob, respectively, and ρ is the density of the fluid), is greater than 3.33×10^3 (at $\mathrm{Re} \approx 3.33 \times 10^3$, the flow is likely to be in the double periodic flow regime [28]). The shear thinning at low shear rates observed in the G2C6G2 micelle solution suggests that larger micelle clusters are relatively weakly held together, and can thus be disrupted to some extent under moderate shear. To demonstrate consistency with other measurements, the steady shear viscosity data were further quantitatively analyzed as follows. The hydrodynamic volume fraction of the micelle clusters (ϕ) can be estimated using Einstein's equation of viscosity [29]

$$\eta = \eta_o(1 + 2.5\phi) \tag{6}$$

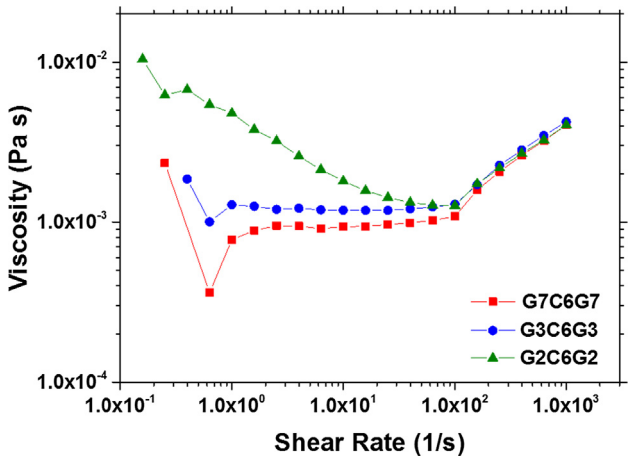

Fig. 8. Shear rate dependent steady shear viscosities of 1.0 wt% G7C6G7, G3C6G3 and G2C6G2 micelle solutions in water at 25 ℃.

where η_o is the viscosity of the solvent (water). The cluster volume fraction is further related to the number and hydrodynamic radius of the micelle clusters containing N micelles (n_N and R_N, respectively) by

$$\phi = \frac{4}{3}\pi R_N^3 \cdot \left(\frac{n_N}{V}\right) \tag{7}$$

where V is the system volume. Assuming that the micelle clusters are reaction-limited colloidal aggregates [30], R_N is related to the hydrodynamic radius of the isolated micelles, R_1 (≈13.75 (=11.9 + 3.7/2), 13.95 (=12.1 + 3.7/2) and 14.55 (=12.7 + 3.7/2) nm for G7C6G7, G3C6G3 and G2C6G2 micelles, respectively, estimated from the cryo-TEM image shown in Fig. 5(c)), by

$$N = \left(\frac{R_N}{R_1}\right)^{2.1} \tag{8}$$

where N is the number of micelles per cluster; the exponent, 2.1, is the so-called fractal dimension of the micelle cluster (assuming that the micelle clusters are formed by the reaction-limited colloid aggregation mechanism [30]). The total number of micelles in the system

$$n_1 = n_N N \tag{9}$$

which can be estimated using the value of micelle core radius estimated by cryo-TEM analysis ($R_{c,TEM}$, listed in Table 2); the n_1/V values are estimated to be 4.26×10^{14}, 6.27×10^{14} and 5.81×10^{14} per mL of 1.0 wt% solutions of G7C6G7, G3C6G3 and G2C6G2 micelles, respectively. Combining Eqs. (6)–(9) gives

$$R_N = \left[\frac{3(\eta - \eta_o)V}{10\pi\eta_o n_1 R_1^{2.1}}\right]^{1/0.9} \tag{10}$$

in which all parameters on the right-hand side are experimentally measurable. Using the measured values of η (Fig. 8), the R_N values were estimated for G7C6G7, G3C6G3 and G2C6G2 micelles; for G2C6G2, the value of viscosity at the lowest shear rate was used (i.e., $\eta \approx 10.4 \times 10^{-3}$ Pa·s at $\dot{\gamma} = 0.159\ s^{-1}$). The resultant R_N values are listed in Table 2 (as "$R_{h,vis}$"). As shown in the table, the hydrodynamic radii of micelle clusters determined from the shear viscosity data ($R_{h,vis}$) are somewhat greater than the values determined by DLS ($R_{h,DLS}$); this discrepancy is due to the different polymer concentrations used in the two experiments (0.03 wt% for DLS, and 1.0 wt% for rheometry). These results further support that G7C6G7 micelles exist as micelle unimers (or small clusters), whereas G3C6G3 and G2C6G2 micelles form larger clusters ($N \approx 1.11 \times 10^3$ and 2.72×10^6, respectively).

In the case of G2C6G2 micelles, the apparent viscosity reaches (close to) a steady-state, minimum value at a critical shear rate of $\dot{\gamma}_c \approx 63.1\ s^{-1}$. At that condition, the size of the micelle clusters is estimated to be R_N (or $R_{h,vis}$) ≈ 469 nm ($N \approx 1.47 \times 10^3$). The minimum shear force required to break up the original clusters into 1470-mers of G2C6G2 micelles can thus be estimated approximately using the equation [31,32]

$$F_N = \frac{5}{2}\pi\eta_o\dot{\gamma}_c R_N^2 \tag{11}$$

The actual value of this force is calculated to be $F_N \approx 6.87 \times 10^{-14}$N. Further, it is reasonable to expect that the micelle unimer breakup force (F_1) is of the same order as the *N*-mer breakup force ($F_1 \approx F_N$); likely, $F_1 \lesssim F_N$ to be more precise. This experimental estimate for the micelle unimer breakup force is far smaller than its predicted value based on the assumption of PEG bridging ($F_1 \approx 5.75 \times 10^{-9}$N), while it is in reasonable agreement with the value estimated from the van der Waals interaction potential ($F_1 \approx 4.69 \times 10^{-13}$N); in fact, the experimental shear force is smaller than the theoretical van der Waals force, which suggests that the level of shear that can be reached reliably in a Couette rheometer ($\dot{\gamma} < 100\ s^{-1}$) is insufficient to break apart G2C6G2 micelle clusters completely into micelle unimers, and this discussion thus rationalizes the observation that the minimum viscosity obtained with the 1.0 wt% G2C6G2 micelle solution ($\eta \approx 1.27 \times 10^{-3}$ Pa·s at $\dot{\gamma} = 63.1\ s^{-1}$) is somewhat higher than the viscosity of the 1.0 wt% G7C6G7 micelle solution (in which G7C6G7 micelles exist in isolated micellar states) ($\eta \approx 0.914 \times 10^{-3}$ Pa·s at all $\dot{\gamma}$). Overall, the rheology results support that the G2C6G2 micelles stick to each other because of the van der Waals force (strongly operative at the close-approach distance between two short PEG-coated micelles).

4. Conclusions

We developed a new amphiphilic block copolymer, PPEGMA-PPC-PPEGMA, which could replace current polymer surfactants. This PPEGMA-PPC-PPEGMA material has an important characteristic that distinguishes itself from conventional linear PEG-based amphiphilic block copolymers; the hydrophilic PPEGMA block has a branched architecture wherein PEG exists as side chains extending from the backbone of methacrylate units. Because of this unique non-linear architecture, the morphological and conformational properties of self-assembled PPEGMA-PPC-PPEGMA polymers are expected to be different from those of linear PEG-based polymer surfactants.

To explore this hypothesis, three different PPEGMA-PPC-PPEGMA triblock copolymer materials having different PPEGMA block molecular weights and an identical PPC block molecular weight were prepared. The self-assembly behaviors of these polymers, both in bulk micellar solution and at the air–water interface, were investigated. Interestingly, we found that when PPEGMA-PPC-PPEGMA is situated at an aqueous interface, only the PEG side chains become hydrated and extended into the aqueous phase, while the PMA backbone remains unhydrated in the interfacial region in contact with the hydrophobic domain formed by PPC. At the air–water interface, this unexpected conformational behavior of PPEGMA-PPC-PPEGMA is manifested in surface pressure-area compression isotherms as the appearance of a second surface pressure plateau at high compression. In micellar situations, the partial hydration of the PPEGMA blocks has important consequences. At all copolymer compositions examined (w_{PEG} = 0.62, 0.41 and

0.37), PPEGMA-PPC-PPEGMA micelles were found to have a spherical geometry, which is in contrast to what has been observed for conventional linear PEG-based amphiphilic block copolymers; at these PEG compositions, linear PEG-based polymer surfactants of comparable molecular weights have been shown to predominantly form spheres, cylinders, and vesicles, respectively [3,6,7]. Because of the small thickness of the PEG corona layer, PPEGMA-PPC-PPEGMA micelles are allowed to approach each other within a relatively small distance; micelles with sparsely grafted PEG chains may even approach each other to a close enough proximity that the van der Waals force takes over and they become (weakly) clustered together.

We suspect that in PPEGMA-PPC-PPEGMA systems, because of the partial hydration of PPEGMA, the micelle geometry is not controlled by the overall PEG weight fraction (as previously discovered in conventional linear PEG-based polymer surfactants [3,6,7]), but instead it is primarily controlled by the PEG weight fraction within the PPEGMA block. This new notion warrants further investigation, particularly given that the PPEGMA chemistry is becoming increasingly popular as the hydrophilic component for amphiphilic block copolymers.

CRediT authorship contribution statement

Jaewon Lee: Methodology, Formal analysis, Investigation, Data curation, Writing - original draft, Visualization. **Jingyi Pan:** Investigation, Visualization. **Jaehun Chun:** Formal analysis, Writing - review & editing. **You-Yeon Won:** Conceptualization, Formal analysis, Writing - review & editing, Supervision, Project administration.

Acknowledgements

YYW is grateful for funding from NSF (CBET-1264336, IIP-1713953, and CBET-1803968) and from ACS PRF (602033-ND7). The authors also acknowledge support from the Purdue University Center for Cancer Research (PCCR) via an NIH NCI grant (P30 CA023168), which supports the campus-wide NMR shared resources that were utilized in this work. JC is grateful for support from DOE-BES/DMSE.

Appendix A. Supplementary material

Supplementary data to this article can be found online at https://doi.org/10.1016/j.jcis.2020.01.080.

References

[1] P. Alexandridis, B. Lindman, Amphiphilic Block Copolymers: Self-Assembly and Applications, Elsevier Science, Amsterdam, The Netherlands, 2000.
[2] M. Ashjari, S. Khoee, A.R. Mahdavian, R. Rahmatolahzadeh, J. Mater. Sci.-Mater. Med. 23 (2012) 943.
[3] S. Jain, F.S. Bates, Macromolecules 37 (2004) 1511.
[4] Y.Y. Won, H.T. Davis, F.S. Bates, Macromolecules 36 (2003) 953.
[5] Y.Y. Mai, A. Eisenberg, Chem. Soc. Rev. 41 (2012) 5969.
[6] D.E. Discher, A. Eisenberg, Science 297 (2002) 967.
[7] Y.Y. Won, F.S. Bates, Giant Micelles: Properties and Applications, CRC Press, 2007, p. 417.
[8] Y.Y. Won, A.K. Brannan, H.T. Davis, F.S. Bates, J. Phys. Chem. B 106 (2002) 3354.
[9] A.V.G. Ruzette, P.P. Soo, D.R. Sadoway, A.M. Mayes, J. Electrochem. Soc. 148 (2001) A537.
[10] H. Lee, J. Lee, J. Park, T. Kwon, S. Hong, Y.Y. Won, Polym. Degrad. Stab. 120 (2015) 149.
[11] J. Lee, S.D. Jo, H. Chung, W. Um, R. Chandrasekar, Y.H. Choi, V.M. Shalaev, Y.Y. Won, ACS Appl. Mater. Interfaces 10 (2018) 26084.
[12] G. Kim, M. Ree, H. Kim, I.J. Kim, J.R. Kim, J.I. Lee, Macromol. Res. 16 (2008) 473.
[13] S. Sudevan, J.K. Min, J.E. Seong, S.J. Na, B.Y. Lee, Angew. Chem. Int. Ed. 47 (2008) 7306.
[14] S. Sujith, J.K. Min, J.E. Seong, S.J. Na, B.Y. Lee, Angew. Chem. Int. Ed. 47 (2008) 7306.
[15] Y.S. Qin, L.J. Chen, X.H. Wang, X.J. Zhao, F.S. Wang, Carbohydr. Polym. 84 (2011) 329.
[16] H.C. Kim, H. Lee, H. Jung, Y.H. Choi, M. Meron, B.H. Lin, J. Bang, Y.Y. Won, Soft Matter 11 (2015) 5666.
[17] H.C. Kim, Y.H. Choi, W. Bu, M. Meron, B.H. Lin, Y.Y. Won, PCCP 19 (2017) 10663.
[18] H.W. Park, J. Choi, K. Ohn, H. Lee, J.W. Kim, Y.Y. Won, Langmuir 28 (2012) 11555.
[19] D.J. Kuzmenka, S. Granick, Macromolecules 21 (1988) 779.
[20] H.C. Kim, H. Lee, J. Khetan, Y.Y. Won, Langmuir 31 (2015) 13821.
[21] H. Lee, D.H. Kim, H.W. Park, N.A. Mahynski, K. Kim, M. Meron, B.H. Lin, Y.Y. Won, J. Phys. Chem. Lett. 3 (2012) 1589.
[22] B.H. Cao, M.W. Kim, Faraday Discuss. 98 (1994) 245.
[23] Y.Y. Won, Korean J. Chem. Eng. 21 (2004) 296.
[24] R.J. Stokes, D.F. Evans, Fundamentals of interfacial engineering, Wiley-VCH, New York, 1997.
[25] P.J. Lu, E. Zaccarelli, F. Ciulla, A.B. Schofield, F. Sciortino, D.A. Weitz, Nature 453 (2008) 499.
[26] S.M. Aharoni, Macromolecules 16 (1983) 1722.
[27] P.G. Degennes, Adv. Colloid Interface Sci. 27 (1987) 189.
[28] R.B. Bird, W.E. Stewart, E.N. Lightfoot, D.J. Klingenberg, Introductory Transport Phenomena, John Wiley & Sons, 2015.
[29] M. Mooney, J. Colloid Sci. 6 (1951) 162.
[30] M.Y. Lin, H.M. Lindsay, D.A. Weitz, R.C. Ball, R. Klein, P. Meakin, Nature 339 (1989) 360.
[31] Y.Y. Won, S.P. Meeker, V. Trappe, D.A. Weitz, N.Z. Diggs, J.I. Emert, Langmuir 21 (2005) 924.
[32] M.C. Dubois-Clochard, J.P. Durand, B. Delfort, P. Gateau, L. Barre, I. Blanchard, Y. Chevalier, R. Gallo, Langmuir 17 (2001) 5901.
[33] S. Kawaguchi, G. Imai, J. Suzuki, A. Miyahara, T. Kitano, Polymer 38 (1997) 2885.